AADE-22-FTCE-078

Real-Time Drilling Hydraulics Advisory System: A Case Study

Ali Karimi, Jonathan Lightfoot, Qian Li, Reza Asgharzadeh, and Tatiana Gobert, Oxy

Abstract

Hydraulics modeling is an essential part of well planning and drilling operations. The ability to monitor hydraulic parameters in (near) real time and make informed decisions can help avoid drilling problems such as poor wellbore cleaning, stuck pipe, lost circulation, trouble running casing to total depth, etc. In this paper we present a powerful tool that leverages real-time drilling data and advanced hydraulic models to obtain and monitor crucial hydraulic parameters.

First, all the required input parameters across several databases are obtained in an automated fashion, then real-time data are passed through a rig-state algorithm to tag each data point for the modeling step. A comprehensive hydraulics model was developed to obtain the system frictional pressure drop and equivalent circulating density during circulation and tripping. Furthermore, a cuttings transport model was developed to determine the minimum required flow rate to clean the wellbore as a function of rate of penetration. Model outputs are validated against an offline industry standard software package. Mud motor efficiency is also calculated and monitored in real time. A database was created to store all the mud motor specifications currently used within the company.

A case study will illustrate how this advisory system was used in action to predict the current and upcoming equivalent circulating density (ECD) and standpipe pressure, optimize tripping operations, and monitor cleanup cycles to ensure efficient wellbore cleaning. This methodology revealed a significant potential to streamline drilling operations, thereby enhancing rig safety and reducing non-productive time.

Introduction

A variety of hydraulic planning software packages are used extensively in the industry today. Although very helpful in the planning stage for a wellbore, the results have to be updated frequently while drilling due to constant changes in the operational parameters (e.g., change in the mud properties or circulation rates). This is a very cumbersome task that can be facilitated by automation. In addition, monitoring the hydraulic parameters in (near) real time can provide valuable information and prevent several drilling problems, such as stuck pipe, lost circulation, motor failures, washouts, and wellbore instability. A circumstantial review of rheological model theory, key equations, and practical data inputs essential in drilling hydraulic modeling applications is included in this paper along with a case study with a modern oil and gas directional drilling assembly.

The goal of this paper is to provide practical knowledge, keen insight, and proven engineering practices related to advanced hole condition monitoring. Calculated estimates of surface flowing pressure while drilling are quite complicated, as demonstrated from the complex theory and mathematical models reviewed. Many factors exist that affect, to a varying degree, the consistency in surface circulating pressure while drilling. The pressure fluctuations in most applications occur when varying torque demands are needed to rotate the drill bit as weight on bit (WOB) is applied. The increase in a fixed-cutter bit's depth of cut (DOC) requires increased torque from both the drill string at the surface and the downhole drilling motor, often called a positive displacement motor (PDM) or mud motor. There are also other scenarios that can cause drilling pressure to fluctuate erratically, such as flow restrictions in the string from debris or failed components. An example is bit nozzle plugging caused by failed elastomers within the bottomhole assembly (BHA). Similarly, there may be erratic flow in the annulus from a packoff or from a hole in the string. A hole in the pipe body or connection, referred to as a washout, is where the pressure declines rapidly as the hole diameter increases, often leading to a pipe failure. Detecting pressure dysfunctions like washouts and unexpected pressure increases while drilling is critical for operational success.

A key aspect of this paper is to explore a past catastrophic event where near-real-time advanced hole condition monitoring could have helped the drilling crew identify the serious deteriorating condition of the borehole circulation system that resulted in equipment being lost in the hole. This case study includes a complex rotary steerable system (RSS) PDM directional drilling BHA system, placing a straight mud motor above the RSS to provide additional torque and rotation in the BHA to increase overall bit RPM and drilling performance.

This paper explores the theory and relationship of the advanced hydraulics model. The featured case study in this paper provides clear evidence to support the use of a relationship between pressure fluctuation and changes in torque, which is a direct result of changes in hookload. This relationship is explored for a catastrophic loss of equipment scenario. The case study provides an excellent example of how

real-time pressure modeling is vital to overall drilling success. Hookload, torque, and pressure are intertwined measurements and are the key to proper monitoring of hole conditions. Data analysis methods described in this paper should not be used in silos, i.e., independently. Drilling analysis is vastly improved when calibrated data charts containing dynamic physics-based models are used systematically. The scenario described will help provide a comprehensive representation of how to use actual "on-bottom" drilling data when conducting torque, drag, and pressure monitoring.

Background

The importance of monitoring hydraulic parameters in real time to reduce drilling problems and improve efficiency has been addressed by several authors. Zoellner et al. (2011) emphasized the importance of real-time hydraulic monitoring and how it can potentially reduce lost time and minimize drilling problems. Borjas and Martibez (2012) presented the idea of preventive workflow in addition to reactive workflows for real-time monitoring. Shahri et al. (2018) showed the possible applications of a steady-state hydraulic model in real time. Porter et al. (2019) addressed the importance of real-time measurements for better accuracy in ECD estimations. Fruhwirth et al. (2006) showed the potential of a neural network approach to model the hydraulic behavior in a well. Reitsma (2005) addressed how combining a real-time hydraulics model and automated choke can be used to maintain a relatively constant bottomhole pressure. Zhang et al. (2016) introduced a transient solid-liquid two-phase flow modeling approach that was applied for real-time drilling hydraulics and cuttings transport calculations.

Although real-time hydraulics is not a new topic, none of the prior publications discussed step-by-step implementation of the model or how it could be used to avoid failures with a realistic case study, which is the main goal of this paper.

Theory

In this section, the applied models to develop the real-time hydraulics tools are discussed. These models include the rheological models, fluid flow in pipes and annulus, surge and swab, wellbore cleaning, motor performance, and tool joint effects. The rig state algorithm and input data automation are also discussed.

Rheological Model

Drilling fluid rheological parameters are the most crucial inputs for hydraulic modeling. Although these parameters are not usually reported explicitly, rotational viscometers readings are available and are saved in the company database several times a day. The most commonly used rheological models for drilling applications include the linear two-parameter Bingham Plastic model, the non-linear two-parameter Power Law model, and the non-linear three-parameter Yield Power Law (YPL) model. Usually, the three-parameter YPL model (proposed by Herschel and Bulkley in 1926), can mimic the rheological behavior of drilling fluids better, so it was used in this work to define the rheological characteristics of the drilling fluids:

$$\tau = \tau_y + K(-\frac{dv}{dr})^m \tag{1}$$

where τ_y is the yield stress, K is the consistency index, and m is the fluid behavior index. Curve fitting techniques are used to obtain the three parameters (τ_y, K, m).

When yield stress is negligible or zero, the YPL model reduces to the Power Law model. Additionally, when m is equal to one, the YPL model reduces to the Bingham Plastic model. The YPL model has been used extensively in the petroleum industry (Kelessidis et al. (2007 and 2011); Hemphill et al. (1993); Mehrabi et al. (2012); Zamora and Slatter (2005); Erge et al. (2015 and 2016); Karimi et al. (2015 and 2016); Gul et al. (2019 and 2020)). Methods are also introduced to obtain the rheological parameters from a pipe viscometer (Karimi et al. (2016), Gul et al. (2020)), which could potentially result in more accurate results because the drilling fluid parameters are measured continuously.

Fluid Flow in Pipes

The following equation represents the relationship between the wall shear stress, τ_w, and pressure loss, $\frac{dp}{dl}$, in a circular pipe:

$$\frac{dp}{dl} = \frac{4\tau_w}{D} \tag{2}$$

Therefore, in order to calculate pressure loss, one needs to obtain the wall shear stress. It can be shown that for 1D, steady-state, fully developed, incompressible, isothermal flow of time-independent YPL fluids with no slip at the wall, wall shear stress can be obtained from the following equation (Ahmed and Miska, 2009):

$$\frac{8v}{D} = \frac{(\tau_w - \tau_y)^{\frac{1+m}{m}}}{K^{\frac{1}{m}}\tau_w^3}\left(\frac{4m}{3m+1}\right)\left[\tau_w^2 + \frac{2m}{1+2m}\tau_y\tau_w + \frac{2m^2}{(1+m)(1+2m)}\tau_y^2\right] \tag{3}$$

Note that Eq. 3 is only valid for laminar flow. Wall shear stress can be obtained numerically from this equation. Keep in mind that Eq. 3 can also be used for Newtonian, power law, and Bingham-plastic fluids. The next step is to determine the flow regime. When wall shear stress is known, Reynolds number can be obtained from the following equation:

$$Re = \frac{8\rho v^2}{\tau_w} \tag{4}$$

where v is the average velocity of the fluid, obtained from:

$$v = \frac{\mathrm{Q}}{A} \tag{5}$$

To determine the critical Reynolds number and characterize transitional flow, the following equations are used:

$$Re_1 = 3250 - 1150N \quad (6)$$

$$Re_2 = 4150 - 1150N \quad (7)$$

where N is the generalized flow behavior index obtained from Eq. 8a.

$$\frac{1}{N} = A + B \quad (8a)$$

where A and B are obtained from the following equations:

$$A = \frac{(1-2m)\tau_w + 3m\,\tau_y}{m\left(\tau_w - \tau_y\right)} \quad (8b)$$

$$B = \frac{2m(1+m)\left[(1+2m)\tau_w^2 + m\,\tau_y\,\tau_w\right]}{m(1+m)(1+2m)\tau_w^2 + 2m^2(1+m)\tau_w\,\tau_y + 2m^3\,\tau_y^2} \quad (8c)$$

When the Reynolds number is lower than Re_1 (Eq. 6), the flow regime is assumed to be laminar. In this case, the friction factor can be obtained from Eq. 9 using the pressure loss from Eq. 2.

$$f = \frac{16}{Re} \quad (9)$$

When the Reynolds number is larger than Re_2 (Eq. 7), the flow regime is assumed to be turbulent and Eq. 10 (Dodge and Metzner, 1959) is applied to obtain the friction factor.

$$\frac{1}{\sqrt{f}} = \frac{4}{N^{0.75}}\log\left(Re \times f^{\left(1-\frac{N}{2}\right)}\right) - \frac{0.4}{N^{1.2}} \quad (10)$$

Wall shear stress must then be recalculated for turbulent flow using Eq. 11. The recalculated wall stress is replaced in Eq. 2 to obtain the pressure loss.

$$\tau_w = \frac{f\rho v^2}{2} \quad (11)$$

For the transitional flow regime (with a Reynolds number between Re_1 and Re_2), an averaging technique is used to obtain the friction factor.

Fluid Flow in Annulus

For modeling the fluid flow of non-Newtonian drilling fluid in the annulus, the narrow slot approximation is used as it presents an acceptable estimation when the diameter ratio (pipe outer diameter ÷ annulus inner diameter) is larger than 0.5.

$$\frac{dp}{dl} = \frac{4\tau_w}{D_{annuls\_id} - D_{pipe\_od}} \quad (12)$$

Like the pipe flow, wall shear stress can be obtained numerically from Eq. 13a:

$$\frac{12v}{D_{OD} - D_{ID}} = \frac{\left(\tau_w - \tau_y\right)^{\frac{1+m}{m}}}{K^{\frac{1}{m}}\tau_w^3}\left(\frac{3m}{1+2\mathrm{m}}\right)\left[\tau_w + \frac{m}{1+m}\tau_y\right] \quad (13a)$$

The generalized flow behavior index, N, can be obtained from the following equations:

$$N = \frac{\mathrm{m}\,C_{ca}}{1 + 2m(1 - C_{ca})} \quad (13b)$$

where x and C_{ca} are obtained from the following equations:

$$x = \frac{\tau_y}{\tau_w} \quad (13c)$$

$$C_{ca} = 1 - \frac{x}{1+m} - \frac{mx^2}{1+m} \quad (13d)$$

The Reynolds number can be obtained from the following equation:

$$Re = \frac{12\rho v^2}{\tau_w} \quad (14)$$

To determine the flow regime, Eqs. 6 and 7 can be used. The flow regime is assumed to be laminar. The friction factor for laminar flow (when the Reynolds number is lower than Re_1) can be obtained from Eq. 15:

$$f = \frac{24}{Re} \quad (15)$$

For turbulent flow, Eq. 10 (Dodge and Metzner, 1959) can be used to obtain the fiction factor. In addition, for the effect of pipe eccentricity in the annulus, the following equations can be used for laminar and turbulent flow accordingly.

Because pipe eccentricity can have a significant impact on pressure loss in horizontal wells with long laterals, the correlation proposed by Haciislamoglu and Langlinais (1990) was used (Eq. 16). This correlation is valid for fluid with behavior index ranging from 0.4 to 1.0. It relates the pressure in an eccentric annulus to a concentric one for laminar (Eq. 16) and turbulent flow (Eq. 17).

$$\left(\frac{dp}{dl}\right)_{ecc.} = \left(1 - 0.072\kappa^{0.8454}\frac{e}{N} - 1.5e^2\kappa^{0.1852}\sqrt{N} + 0.96e^3\kappa^{0.2527}\sqrt{N}\right)\left(\frac{dp}{dl}\right)_{con.} \quad (16)$$

$$\left(\frac{dp}{dl}\right)_{ecc.} = \left(1 - 0.048\,\kappa^{0.8454}\frac{e}{N} - 0.67e^{2}\kappa^{0.1852}\sqrt{N} + 0.28e^{3}\kappa^{0.2527}\sqrt{N}\right)\left(\frac{dp}{dl}\right)_{con.} \quad (17)$$

Surge and Swab Model

During the tripping operation, pressure increase (surge pressure) and decrease (swab pressure) must be accounted for in a comprehensive hydraulic model. Usually, the maximum surge/swab pressure is anticipated when the bottom of the pipe is closed (e.g., plugged nozzle or one-way float valve). Therefore, the equations used here are for a closed-end pipe and provide conservative assumptions for tripping speeds.

Since the equations for surge and swab calculations are complex for real-time applications, a simplified technique presented by Burkhardt (1961) is used. In this approach, the mean annular velocity, v_{ae}, is defined by Eq. 18:

$$v_{ae} = v + \alpha\, v_p \quad (18)$$

where v_p is the pipe velocity (positive or negative for tripping in and out, respectively), and α is the mud clinging constant that can be obtained from Eqs. 19a and 19b for laminar and turbulent flow, respectively.

$$\alpha_{lam} = \frac{\kappa^2 - 2\kappa^2 - \ln(\kappa) - 1}{2(1-\kappa^2)\ln(\kappa)} \quad (19a)$$

$$\alpha_{tur} = \frac{\sqrt{\frac{\kappa^4 + \kappa}{1+\kappa}} - \kappa^2}{(1-\kappa^2)} \quad (19b)$$

The mean annular velocity, v, for the closed-end pipe can be obtained from Eq. 20:

$$v = \frac{D_{pipe\_od}^2 v_p}{D_{hole\_id}^2 - D_{pipe\_od}^2} \quad (20)$$

Then, to calculate the pressure loss in the annulus, the equations presented in the previous section can be applied.

Pressure Loss Across the Bit

By ignoring the viscous frictional effects through short nozzles, the following equation (Eq. 21) is used to obtain the pressure loss across the bit:

$$\Delta p_{bit} = \frac{\rho q^2}{2C_d^2 A_t^2} \quad (21)$$

Effect of Tool Joint

In a narrow annulus, pressure loss associated with sudden expansion and contraction (area change) due to the presence of tool joints could be significant and may not be ignored (Karimi et al., 2014). By using Bernoulli's equation for sudden expansion/contraction, one can obtain:

$$P_{exp/cont} = \rho v_{tj}^2 \left(\left(\frac{A_{tj}}{A_{ann}}\right)^2 - 1\right) \quad (22)$$

where v_{tj}^2 is the fluid velocity across the tool joint, and A_{tj} is the annular area due to tool joint presence (which is smaller than the annular area opposite the pipe). Once the tool joint specifications (e.g., outer diameter) are known, v_{tj}^2 and A_{tj} can easily be calculated. The number of tool joints present can be estimated according to pipe length (usually 30 ft joints). Note that Eq. 22 is only for squared tool joints. For tapered tool joints, a correction factor can be used that depends on the tool joint specifications.

Cuttings Transport

To avoid complexity of running a transient cuttings transport model in real-time, a correlation-based approach is used to estimate the minimum flow rate required to clean the wellbore. For the highly deviated and horizontal section (inclination > 55°), Larsen's correlation is used (Larsen et al., 1997). For the vertical and near-vertical section, the correlation proposed by Rubiandini (1999) is used. Interpolation techniques are used to predict the minimum required flow rate for the deviated section when the inclination angle is less than 55° by using both the Rubiandini and Larsen correlations.

Initially, the wellbore is divided into several segments, and the minimum required flow rate is calculated for each segment. Finally, the minimum flow rate required to properly clean the wellbore is reported as the maximum of all the cleaning flow rates across the segments. If the pump flow rate falls below the recommended flow rate, a cuttings bed will be generated, which may cause drilling problems such as stuck pipe or difficulty in running casing.

Mud Motor Performance

Motor efficiency is estimated as a ratio of actual power to expected power (Eq. 23):

$$Motor\ efficiency = \frac{actual\ power}{expected\ power} \times 100 \quad (23)$$

where actual and expected power are defined by Eqs. 24 and 25, respectively:

$$Actual\ power = motor\ torque \times motor\ rpm \quad (24)$$

$$Expected\ power = diff.pressure \times flow\ rate \quad (25)$$

To calculate motor RPM and torque, a model was developed using motor specifications (maximum and stall differential pressure, maximum torque, and revolutions per gallon) and its performance curves. The real-time inputs to the model are mud flow rate and differential pressure from the hydraulics model.

Hydraulic Rig State

To improve the efficiency of the calculations and also give a more detailed breakdown of the hydraulic events, a rule-based

algorithm was developed to determine the state of the time series data in terms of drilling hydraulics. Each data points is assigned to of the following states:

1) On-bottom
    a. Drilling (with circulation)
    b. Circulation only
    c. No circulation
2) Off-bottom
    a. Circulation
    b. No circulation

This detailed breakdown facilitates the troubleshooting for engineers, particularly when the focus is only on a certain part of the operations.

Input Data Automation

One of the most important aspects of running the algorithm in real time is to pull the required input data automatically from the relevant databases. Contextual data required for the algorithm include:

- BHA and mud motor information
- Drilling fluid reports
- Casing depth and size
- Directional surveys

Automated queries have been created to pull information from the reporting system to ensure that the most up-to-date data are used to run the algorithm. It is also possible to override the input data received from the reporting system in case of mistakes in data entry or for sensitivity analysis for planning purposes.

Model Validation

Before applying the proposed models in this work, the results were validated against a widely used software package in the industry.

For simplicity, consider a 10,000 ft well with 4 ¾-in. hole and 3 ½-in. drillpipe. Such a slimhole configuration enables us to investigate the effect of the tool joint on annular pressure loss, which is more prominent is slim holes or narrow clearances. Additional information used for the simulations, including the hole size, bit size, and drilling fluid properties, is provided in **Fig. 1**.

In first part of the validation, pressure losses in the drillstring, annulus, bit, and the entire system were compared with the commercial software. Initially, the effect of the tool joint was not considered. **Fig. 2** compares the pressure drop in different segments (drillstring, annulus, bit, and system) for this example. The points present the results obtained from the models described in the previous section, and the solid lines present the results from the commercial software. **Fig. 2** shows there is excellent agreement between the results obtained from the model and the commercial software. To consider the effect of the tool joint, it was assumed that the connection ID is the same as the pipe ID, 2.992 in., while the connection OD was 4.406 in. **Fig 3**. shows the pressure loss in the different components. As anticipated, the pressure loss in the annulus and the entire system increased significantly due to the presence of tool joints. **Fig. 3** also indicates that in the presence of tool joints there is still an excellent match between the model and the industry standard software.

The validation of surge and swab results was conducted by comparing the results from the model with the widely used software. **Fig. 4** shows the surge and swab pressure in terms of Equivalent Circulating Density (ECD) vs. pipe movement speed, which is presented in terms of time required to move one stand in or out. It was assumed that each stand is 90 ft long. The markers present the results from the model, and the solid line presents the results from the industry software. **Fig. 4** shows very good agreement between the two results, particularly in the operational zone. The slight discrepancy observed at the beginning of the graph, when time per stand is low (i.e., the pipe is moved quickly) may be explained by differences in the annular frictional loss model in the turbulent regime. In addition, very good agreement was also observed in comparison with models proposed by Erge et al. (2018) and He et al. (2016), which is beyond of scope of this work.

Case Study

To understand this case study better, we will review some basic definitions and the functionality of some drilling equipment. Downhole motors have two primary directional drilling applications: bent-housing steerable motors, and the motor-powered rotary steerable system (RSS). In the RSS application, the motor housing is straight or set to 0° for only rotary drilling. In the bent-housing application, the motor is rotated for tangent drilling and slid for steering intervals to achieve necessary well objectives and the required trajectory. In both applications, a downhole motor supplies additional energy downhole by both increasing the bit rotational rate and providing additional downhole torque near the bit. In addition to applied WOB, motors require the use of differential pressure, also known as ΔP_{motor}, as a key operational parameter. In this case, the difference is the increase in pressure experienced between off-bottom circulation and on-bottom circulation (while drilling). In general, torque output of a motor has a near-linear relationship to the increase in ΔP_{motor}. However, the speed of a motor declines—often rapidly—as ΔP_{motor} increases. This rate of decline increases significantly as flow rate declines, and when a motor reaches zero rotations per minute (RPM), the motor stalls and is no longer able to rotate.

Torque and drag analysis (TDA) is often used to describe hole condition monitoring, but often the TDA workflow tracks non-drilling off-bottom activity. TDA plots pick-up or slack-off string hookloads against broomstick plots in addition to tracking off-bottom torque against modeled torque, all with varying friction factors. These charts are commonly called TDA broomsticks. Traditional TDA workflows have not included actual on-bottom drilling surveillance. Obviously, off-bottom pick-up, slack-off and rotating torque while tripping or making connections is not truly a drilling activity. This work happens between drilling stands or while tripping the assembly.

In recent years, the industry has included actual on-bottom drilling data. Hookload torque and pressure surveillance matched with dynamic physics-based models is a key activity

while using full drilling parameters such as ideal drilling rotation speed, torque, WOB, ΔP_{motor}, desired penetration rates, and necessary flow rates. Note that surface WOB is not commonly measured directly. WOB is a differential hookload, (ΔHL), between off-bottom rotational hookload, commonly called free-hanging weight. The reduction in surface hookload when surface tension is released affects the bit weight, which starts as the bit contacts the bottom of the borehole. At this time the bit weight and differential pressure are set to a tare value of zero, commonly called the zero set point (ZSP).

Setting the ZSP is a key human-factors event in drilling. It is not uncommon for the ZSP to be set with gross error. WOB and ΔP_{motor} depend on a valid tare to be accurate and should be set while rotating off-bottom without a motor torque load and without linear string movement. Rotational weight off-bottom is easy to model and typically only changes with flow rate and mud density while drilling a lateral interval. Adding the WOB to hookload data curves while on-bottom drilling provides a real-time calculated curve that can be easily compared to the broomstick model curve for rotating off-bottom to ensure that ZSP for the *ΔHL* (WOB) used is valid. The off-bottom curve is typically the center line of the broomstick chart between pick-up and slack-off curve fanned with varying friction factors.

This method is much easier with an RSS assembly because rotational drag is minimized when applying weight to the bit. Although, assembly drag while slacking off can be significant due to complex borehole tortuosity, extended reach, or other complex well shapes, it should be considered in this case. While sliding with a bent-housing motor, drillstring assembly drag can be significant, making the process of setting up a good ZSP much more complicated. This method of setting the ZSP is further complicated when the pipe is oscillated by the rig from the surface to break friction while slide steering.

In recent years, machine learning algorithms and automated controls have worked to reduce the impact of manual zero setting; however, it is common to experience significant differential hookload and pressure error with automated zeroing systems. It is important to validate WOB (ΔHL) and ΔP_{motor} to ensure the basis for the zero being used does not defy the laws of physics and the rule of common sense.

While drilling a lateral section of a horizontal well, the WOB should added to the measured hookload while drilling. This curve should be compared to the physics-based model of the rotational off-bottom weight, traditionally the center line between the pick-up and slack-off curves of a broomstick chart. This calculated off-bottom zero hookload should match the calibrated rotational weight model. The curve should only change in a linear fashion as the well is deepened as long as the fluid density and flow rate remain constant. If the key parameters change, the model should be adjusted and recalibrated to establish a new comparison model. In addition, this practice of a normalized hookload (NHL) comparison can be directly used to calculate the degree of bit weight error applied by rigsite personnel or computer control systems. This method of using NHL often provides a clear picture when penetration rates are lower than expected, often caused by an actual lower WOB and DOC. Likewise, high torque is often better understood when the actual calculated WOB is higher than expected. In recent years, downhole strain-gauge axial load bit weight sensors have clearly demonstrated a significant opportunity for vast improvements of bit weight estimates using only surface data and the human- or machine-selected ZSP.

In similar fashion, the ΔP_{motor} can be subtracted from the drilling standpipe pressure measurement, establishing a calculated off-bottom normalized pressure curve (NPC) while drilling. The NPC can easily be compared to the off-bottom physics-based modeled pressure, thereby removing the bit-motor interaction. In general, the pressure will increase in a linear fashion when consistent flow rates and mud properties are used as the length of pipe increases. Pressure drops are typically steady and consistent in the bit nozzles, BHA components, drill string, surface equipment, and annulus. The primary change in surface pressure while drilling the openhole interval is the length of pipe. The overall off-bottom pressure gradually increases as the bit drills deeper into the wellbore. Individual assemblies and hole sections must be modeled and calibrated at the start of the interval to provide a linear forecast of pressure as the pipe is lengthened. The real-time normalized calculated drilling pressure minus the ΔP_{motor} curve provides clear evidence of a valid ΔP_{zero} and provides a better hole condition monitoring (HCM) surveillance curve to compare with the hydraulics model. After recalibration, the advanced real-time hydraulics model can be adjusted using real-time inputs of fluid density, rheology, and cuttings loading. Comparison of a dynamic pressure model with a normalized pressure curve will provide a clear indication of drilling hydraulic dysfunctions such as a string washout or an annular restriction or pack-off while drilling.

Another key drilling parameter used to compare on-bottom surface loads to a model is the torque while drilling. Torque is sensitive to both friction and bit weight. Tracking the differential torque $\Delta Torque$ between on-bottom and off-bottom is another key parameter for advanced HCM. Torque output of a motor is linearly related to ΔP_{motor}. Therefore, the additional torque provided by the motor can easily be estimated. However, drillstring side-loading increases as the length of string compression increases. A physics-based model of expected torque should include and be adjusted by actual bit weight, fluid properties, flow rate, and differential pressure. In addition, the depth-based average torque (1-ft average) and time-based torque (1-sec actual) is important for HCM. Both curves used together are helpful for providing both normalized average torque and the torque fluctuation or spread. The torque spread at the surface is often referred to as the degree of stick/slip. An increase in stick/slip happens when the torque swings widely or fluctuates. Often the torque swing is erratic in nature, sometimes causing the string to stop. String rotation can reverse direction at the surface in the most severe stick/slip cases. ΔP_{motor} can provide key insight and evidence for unexpected changes in drilling torque and drilling performance.

The case study wellbore in this paper is a Midland Basin

unconventional horizontal well that was drilled with a modern onshore top-drive drilling rig.

After landing the 8 ¾-in. curve, the first horizontal BHA (**Fig. 4**) for the lateral production interval was used. The assembly consisted of an 8 ½-in. PDC bit, 6 ¾-in. point-the-bit RSS, MWD, drilling motor, integral blade stabilizer and 5-in. 19.5-lb/ft S-135 drill pipe with 4 ½-in. IF connections. The complete BHA is only 95 ft long, or 1% of the full string. The drill pipe connecting the BHA to the surface is 13,082 ft long, or 99% of the entire assembly at the point of catastrophic failure. The individual lengths of assembly components are listed in **Table 1**. **Fig. 5a** shows the BHA sketch and directional profile. A 9.4-ppg water-based drilling fluid was used to drill this hole section. **Table 2** shows the drilling fluid viscometer readings.

The drilling motor power section utilized in this assembly was a 7:8 3.0 stage slow-speed (0.15 revolution/gallon) high-torque configuration. The speed range of the motor is 45 to 90 RPM with a corresponding flow rate range of 300 to 600 gal/min (gpm). This type of high-torque power section is a common motor configuration originally designed for air drilling applications. These designs have become popular in recent years for fluid drilling applications because of the overall horsepower generated at low speeds. The power section design produces 12,780 ft-lb of torque at the recommended maximum differential pressure of 750 psi, a ratio of 17.04 ft-lb/psi. The motor stall torque is 25,560 ft-lb, and it can operate at a maximum hydraulic horsepower of 262 hp (Q × ΔP/1714) for the maximum rated flow rate of 600 gpm at 750 psi ΔP. The mechanical horsepower for this motor is approximately 180 hp (RPM × Torque/5252). The RPM at full load declines to roughly 74 from the original 90 RPM at zero ΔP_{motor} load, and the torque output with the motor fully loaded (max ΔP_{motor}) is 12,780 ft-lb. The overall hydraulic to mechanical efficiency for the motor used in this application is 69% (Output Energy / Input Energy × 100%).

A look back at the general time summaries reported for the event offered very little explanation as to what caused the severe drilling dysfunction that ultimately led to equipment being lost in the hole. These are comments from the directional driller report:

"*The motor above the RSS system used 350 - 450 differential pressure and 80 RPM on surface during the entire run without problems. At 13,044 ft the mud motor started stalling with over 1,000 psi of differential, and the torque was 22,000 ft-lb. It is possible that the RSS became stuck, which caused the motor to become stalled. The motor and BHA below the motor were left downhole.*"

The daily report showed that drilling progressed 1,742 ft in 24 hours from 11,435 ft to 13,177 ft with an average penetration rate of 98 ft/hr. The three general time summary comments during this time follow:

1. *00:00 – 20:30 Drilling ahead from 11,435 – 13,177 ft on the lateral section, taking surveys every two stands by drill site manager request and sending downlinks as needed.*

2. *20:30 – 21:00 Noticed that torque started to come up, so client decided to add StarGlide in the system. Driller picked up off bottom and noticed that torque started to go up to 25,000 ft-lb. In addition, differential pressure was up to 1,200 psi. The client drill site manager decided to TOOH (trip out of hole) to check BHA. While pulling the string only 30 ft, the drill string became stuck.*

3. *21:00 – 24:00 Work stuck pipe till wireline arrives to free point.*

The rig crew worked the stuck pipe for two days leading to the decision of using chemical cutters to part the string. Fishing continued unsuccessfully for another four days.

The drilling team made the decision to abandon a part of the original hole section and leave the BHA in the hole. The original interval shown in red in **Fig. 5b** was abandoned at 11,350 ft measured depth, and the new sidetrack lateral (green) was successfully drilled to meet the original planned (blue) depth, and the well objectives were met without further incident.

This well was chosen for this paper as it provides an excellent example of the value of having a dynamic hydraulics model with near-real-time adjustments. The expected drilling pressure calculated with operational inputs such as flow rate, mud weight, fluid properties, and cuttings loading are key to hole condition monitoring. In addition, we need to confirm tare setpoints often for hookload and differential pressure. **Fig. 6** illustrates the concept of normalized hookload while drilling, and the figure caption explains why it is clear that the off-bottom rotating free-hanging weight used while drilling had significant error while drilling this interval.

Similarly, **Fig. 7** proves that normalized drilling pressure from a linear model is not sufficient. The manually updated model using the average fluid density and flow rates proves that pressure models need to be adjusted often while drilling, and in this case, constant changes in fluid properties make it difficult to monitor with traditional linear curves.

Another use for the real-time tool is for lookback studies where we look at past problematic wells and analyze the results in greater detail. This enables us to apply the tool for troubleshooting to avoid future dysfunction events. A digital twin of what is happening in the field could be very helpful to identify deviations from the plan.

Fig. 8 shows the modeled and actual standpipe pressure for this case study. Initially, there is a very good match between the actual and modeled standpipe pressure. However, when the cuttings buildup occurs in the annulus, there are several pressure spikes that cannot be explained by the model (significant discrepancy between the model and actual values).

Fig. 9 shows the minimum required flow rate to clean the wellbore vs. depth (green line), and the pink dots are the flow rates observed in the field (the rig state is used to display only the flow rate data points during the drilling process). This figure shows that by increasing the rate of penetration, the required flow rate to clean the wellbore also increases. However, the flow rates used in the field, even though sufficient for cleaning the wellbore in the vertical section, were considerably below the minimum flow rate needed to clean the wellbore in the curved section properly. This could lead to generation of a significant cuttings bed (especially at high ROP). This may help

explain the high hookloads observed when picking up the string. The solution to this problem could be increasing the flow rate to exceed the minimum required cleaning flow rate.

Fig. 10 shows the ECD and bottomhole pressure vs. flow rate, which indicates it was possible to increase the flow rate to exceed the minimum flow rate required for cleaning the wellbore. However, the applied flow rate in the field was very close to the maximum flow rate ratings of the downhole equipment. Therefore, this was not a viable option. The other option was to change the mud properties to enhance the carrying capacity to remove the cuttings successfully from the wellbore. However, this solution was only applied when the cuttings buildup was significant and the pressure spikes were observed. By creating a digital twin of the operations, it was possible to identify the problem before it posed any threat to the operations.

In addition to having a digital twin of the standpipe pressure and providing wellbore cleaning and flow rate guidelines during drilling, the real-time hydraulic tool can also be used for automated tripping operations. **Fig. 11** shows the ECD while tripping. This figure provides a general guideline for the safe tripping speeds during tripping in or out operations. The pipe movement speed can also be estimated when the tripping connection time is provided. An example of the tripping connection time vs. rig time is shown in **Fig. 12**. Note that a separate algorithm was developed for this purpose (see Karimi et al., 2020), which is also used in the real-time hydraulic application.

Conclusions

- In this study, step-by-step modeling details are provided for a comprehensive hydraulic model with the capability of generating an accurate digital twin. Accurate standpipe pressure, recommended tripping speeds, cuttings transport, and motor efficiency curves are provided in near-real-time for effectual monitoring, sound decision making, and insightful advisory.
- The deployment of this tool could potentially have prevented a stuck pipe incident and the subsequent loss of downhole equipment observed in this long lateral. Clear and present danger indicators would have been presented well before this event occurred.
- The post-well analysis is an excellent application for this robust physics-based drilling model that creates a digital twin of expected drilling circulating pressure. In this case, it was clear that pressure was much higher than expected due to poor hole cleaning, and the resultant wide drilling torque swings were a result of both bit weight error and BHA packoff, which occurred during the final hour of drilling. Stick/slip along with motor stalls clearly indicated a severe drilling dysfunction that led to the decision to pull the string, and the string got stuck shortly thereafter. The remedy would have been to improve fluid rheology and clean the wellbore of cuttings and debris before pulling the string into a wedged tight spot.
- Future work will be to develop a similar tool for adjusting on-bottom drilling hookloads as a function of flowrate and mud density. A review of the drilling data in this study clearly indicates that establishing a similar dynamic hookload model is an equally important exercise. Further work to generate a dynamic normalized hookload model for accurate estimates of downhole drilling loads placed on the bit is clearly needed.

Acknowledgments

The authors would like to thank Oxy for permission to publish this work. In addition, Philippe Haffner, William Turner, Juan Mejia, Reza Banirazi, John Willis, Diego Tellez, Derek Adam, and Dipti Sankpal are acknowledged for their contribution, brainstorming, and assistance with developing the tool. Thanks also go to Jeanne Perdue for editing this paper.

Nomenclature

τ_w = Shear stress at the wall, Pa
τ_y = Yield stress, Pa
N = Generalized flow behavior index
A = Area, m^2
C_d = Bit discharge coefficient
D = Diameter, m
K = Consistency index, $Pa{\cdot}s^m$
Q = Flow rate, m^3/s
Re = Reynolds number
e = Dimensionless eccentricity
f = Friction factor
l = Length, m
m = Fluid behavior index
p = Pressure, Pa
r = Radius, m
v = Velocity, m/s
α = Mud clinging constant
κ = Diameter ratio
ρ = Density, kg/m^3
τ = Shear stress, Pa

Glossary

BHA = *Bottomhole assembly*
DOC = *Depth of cut*
ECD = *Equivalent circulating density*
GPM = *Gallons per minute*
HCM = *Hole condition monitoring*
NHL = *Normalized hookload*
NPC = *Normalized pressure curve*
PDM = *Positive displacement motor*
ROP =*Rate of penetration*
RPM = *Revolutions per minute*
RSS = *Rotary steerable system*
TDA = *Torque and drag analysis*
WOB = *Weight on bit*
ZSP = *Zero setpoint*

References

1. Ahmed, R., Stefan Miska, S.Z. Advanced wellbore hydraulics, chapter 4.1, (pp. 191-219). "Advanced drilling and well technology". USA Society of Petroleum Engineers. Ed. Bernt S. Aadnoy. SPE, 2009.
2. Borjas, Ricardo, Martinez, Leopoldo, Perez, Carlos, and Reginaldo Rodriguez. "Real-Time Drilling Engineering: Hydraulics and T&D Modeling for Predictive Interpretation While Drilling." Paper presented at the SPE Intelligent Energy International, Utrecht, The Netherlands, March 2012. doi: https://doi.org/10.2118/150069-MS
3. Burkhardt, J.A.. Wellbore Pressure Surges Produced by Pipe Movement. J Pet Technol 13 (1961): 595–605. doi: https://doi.org/10.2118/1546-G-PA
4. Dodge, D.W. and Metzner, A.B. 1959. Turbulent Flow of Non-Newtonian Systems. AIChE J. 5 (2): 189–204.
5. Erge, O., Karimi Vajargah, A., Ozbayoglu, M. E., & van Oort, E. (2016, March 1). Improved ECD Prediction and Management in Horizontal and Extended Reach Wells with Eccentric Drillstrings. doi:10.2118/178785-MS
6. Erge, O., Karimi Vajargah, A., Ozbayoglu, M.E., and van Oort, E. Frictional pressure loss of drilling fluids in a fully eccentric annulus, Journal of Natural Gas Science and Engineering, Volume 26, September 2015, Pages 1119-1129.
7. Fruhwirth, Rudolf Konrad, Thonhauser, Gerhard, and Wolfgang Mathis. Hybrid Simulation Using Neural Networks To Predict Drilling Hydraulics in Real Time. Paper presented at the SPE Annual Technical Conference and Exhibition, San Antonio, Texas, USA, September 2006
8. Gul, Sercan , van Oort, Eric , Mullin, Chris , and Douglas Ladendorf. Automated Surface Measurements of Drilling Fluid Properties: Field Application in the Permian Basin. SPE Drill & Compl 35 (2020): 525–534.
9. Gul, Sercan, Johnson, Mitchell David, Karimi Vajargah, Ali , Ma, Zheren , Hoxha, Besmir Buranaj, and Eric van Oort. A Data Driven Approach to Predict Frictional Pressure Losses in Polymer-Based Fluids. Paper presented at the SPE/IADC International Drilling Conference and Exhibition, The Hague, The Netherlands, March 2019.
10. Haciislamoglu, M. and Langlinais, J. 1990. Non-Newtonian flow in eccentric annuli. Journal of Energy Resources, pp 163,169.
11. Hemphill, T., Campos W., Pilehvari A. 1993. Yield-Power Law Model More Accurately Predicts Mud Rheology. Oil & Gas Journal 45.
12. Herschel, W.H., Bulkley, R., 1926. Konsistenzmessungen von Gummi-Benzollosungen. Kolloid Z. 39, 291.
13. Karimi Vajargah, A., van Oort, E., Determination of drilling fluid rheology under downhole conditions by using real-time distributed pressure data, Journal of Natural Gas Science and Engineering, Volume 24, May 2015, Pages 400-411.
14. Karimi Vajargah, Ali , Banirazi, Reza , Pablo Mejia, Juan , and Phillippe Haffner. An Automated Workflow for Real-Time Monitoring and Benchmarking of Connection Time in Drilling Operations. Paper presented at the IADC/SPE International Drilling Conference and Exhibition, Galveston, Texas, USA, March 2020. doi: https://doi.org/10.2118/199616-MS
15. Karimi Vajargah, K., Sullivan, G., & van Oort, E. (2016, September 14). Automated Fluid Rheology and ECD Management. Society of Petroleum Engineers.
16. Karimi, A., Najafi Fard, F., Parsi, M., & Buranaj Hoxha, B. (2014, September 10). Investigating the Impact of the Tool Joint Effect on Equivalent Circulating Density in Deep-Water Wells. Society of Petroleum Engineers. doi:10.2118/170294-MS.
17. Kelessidis, V. C., R. Maglione, C. Tsamantaki and Y. Aspirtakis. 2006. Optimal Determination of Rheological Parameters for Herschel-Bulkley Drilling Fluids and Impact on Pressure Drop, Velocity Profiles and Penetration Rates during Drilling. J. Petrol. Sci. Eng. 53, 203–224 (2006).
18. Kelessidis, Vassilios C., Panagiotis Dalamarinis, and Roberto Maglione. 2011. Experimental Study and Predictions of Pressure Losses of Fluids Modeled as Herschel–Bulkley in Concentric and Eccentric Annuli in Laminar, Transitional and Turbulent flows. Journal of Petroleum Science and Engineering 77 (3): 305-312.
19. Larsen, T. I., Pilehvari, A. A., & Azar, J. J. (1997, June 1). Development of a New Cuttings-Transport Model for High-Angle Wellbores Including Horizontal Wells. Society of Petroleum Engineers. doi:10.2118/25872-PA
20. Mehrabi, M., Zeyghami, M., & Shahri, M. P. (2012, January 1). Modeling of Fracture Ballooning in Naturally Fractured Reservoirs: A Sensitivity Analysis. Society of Petroleum Engineers. doi:10.2118/163034-MS
21. Porter, Aidan , Lie, Vivek , and Joshua Gollapalli. Enhanced Hydraulic Modeling and Event Detection Using Real-Time Fluid Properties and Fluid Position Tracking Software. Paper presented at the SPE Middle East Oil and Gas Show and Conference, Manama, Bahrain, March 2019. doi: https://doi.org/10.2118/194812-MS
22. Reitsma, Don. Development and Application of Combining a Real-Time Hydraulics Model and Automated Choke To Maintain a Relatively Constant Bottomhole Pressure While Drilling. Paper presented at the International Petroleum Technology Conference, Doha, Qatar, November 2005. doi: https://doi.org/10.2523/IPTC-10708-MS
23. Rubiandini R.S., R. (1999, January 1). Equation for Estimating Mud Minimum Rate for Cuttings Transport in an Inclined-Until-Horizontal Well. Society of Petroleum Engineers. doi:10.2118/57541-MS
24. Shahri, Mojtaba , Kutlu, Bahri , Thetford, Taylor , Nelson, Brian , Wilson, Timothy , Behounek, Michael , Ambrus, Adrian , and Pradeepkumar Ashok. Adopting Physical Models in Real-Time Drilling Application: Wellbore Hydraulics. Paper presented at the SPE Liquids-Rich Basins Conference - North America, Midland, Texas, USA, September 2018. doi: https://doi.org/10.2118/191797-MS
25. Zamora, M., Roy, S., Slatter, K., 2005. Comparing a basic set of drilling fluid pressure-loss relationships to flow-loop and field data. Paper AADE-05-NTCE-27. Proceedings of AADE National Technical Conference and Exhibition, Houston (USA).
26. Zhang, F. , Filippov, A. , Jia, X. , Lu, J. , and V. Khoriakov. Transient solid-liquid two-phase flow modelling and its application in real-time drilling simulations. Paper presented at the 10th North American Conference on Multiphase Technology, Banff, Canada, June 2016.
27. Zoellner, P.. , Thonhauser, G.. , Lueftenegger, M.. , and H. F. Spoerker. Automated Real-time Drilling Hydraulics Monitoring. Paper presented at the SPE/IADC Drilling Conference and Exhibition, Amsterdam, The Netherlands, March 2011. doi: https://doi.org/10.2118/140298-MS

Tables

Table 1 – The BHA used for the case study well

Section Type		Length (ft)	OD (in)
Drill Pipe		13,082.26	5.000
Stabilizer		4.91	6.750
Mud Motor		31.14	6.750
Sub		4.93	6.750
MWD		38.35	6.750
Rotary Steerable System		14.86	6.750
Bit		0.85	8.500

Table 2 – Rotational viscometer readings for the drilling fluid

RPM	readings
600	18
300	14
200	12
100	9
6	5
3	4

Figures

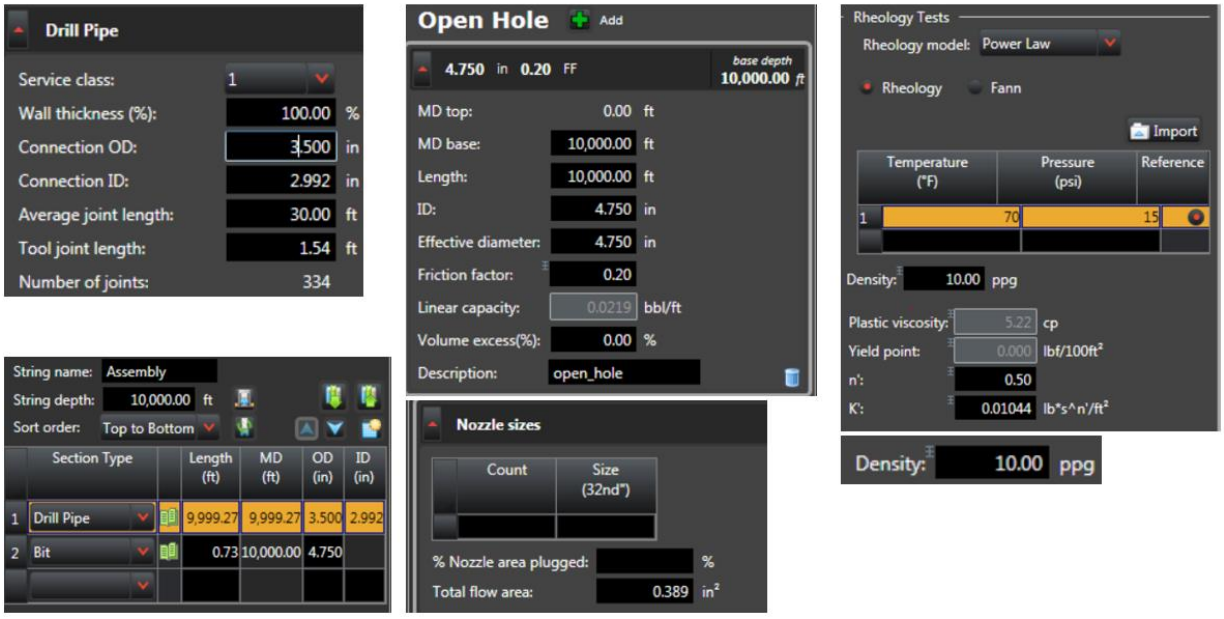

Figure 1 – Input data for the validation case

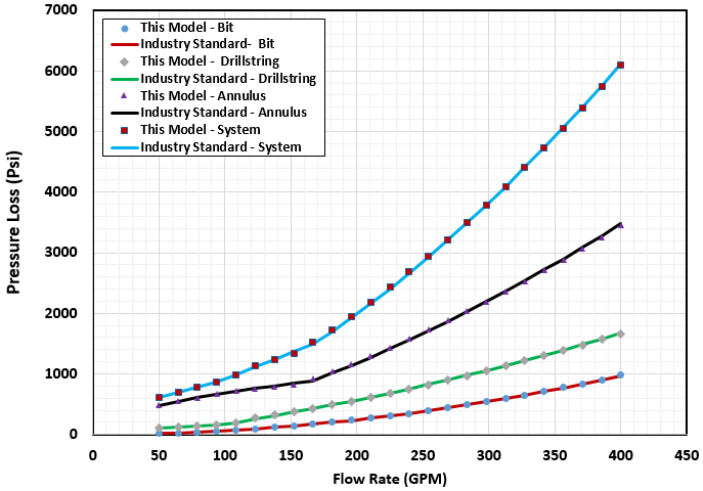

Figure 2 – Comparison of pressure loss in drillstring, annulus, bit, and system for the model presented here against the industry standard software (tool joint effect is ignored).

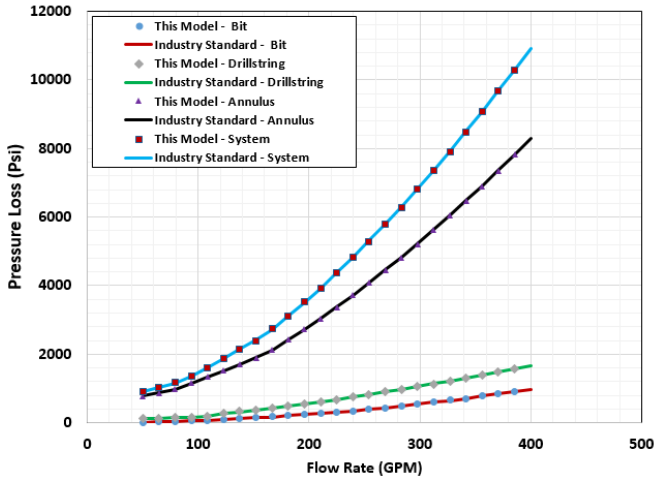

Figure 3 – Comparison of pressure loss in drillstring, annulus, bit, and system for the model presented here against the industry standard software (tool joint effect is considered).

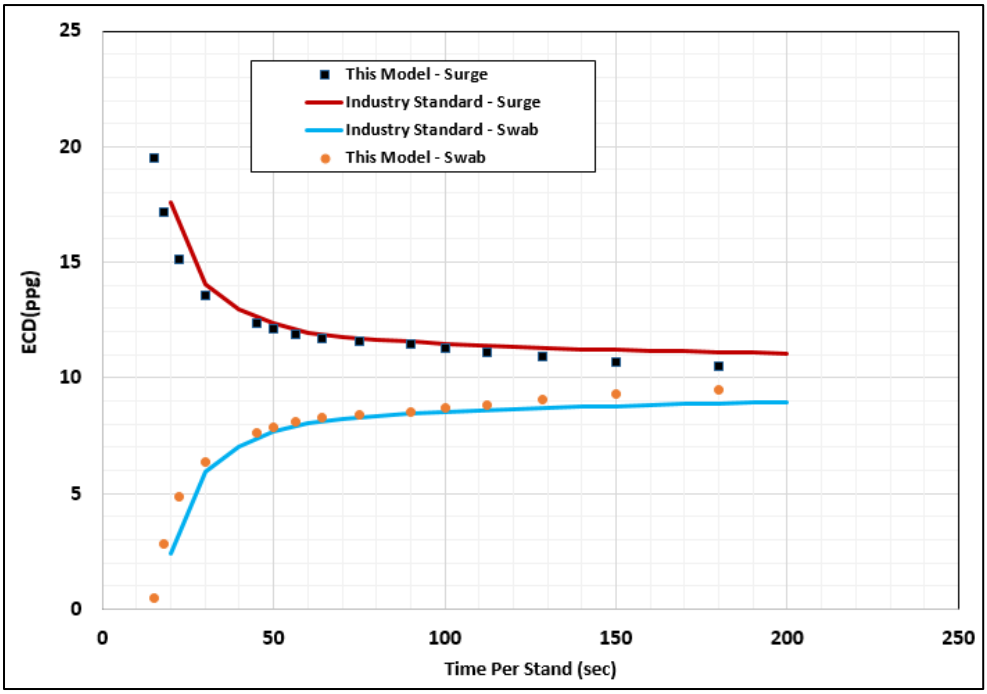

Figure 4 – Comparison of ECD change due to surge and swab between this work and commercial software. Static mud weight is 10 ppg. Time per stand is the time it takes to move one stand (90 ft in this work).

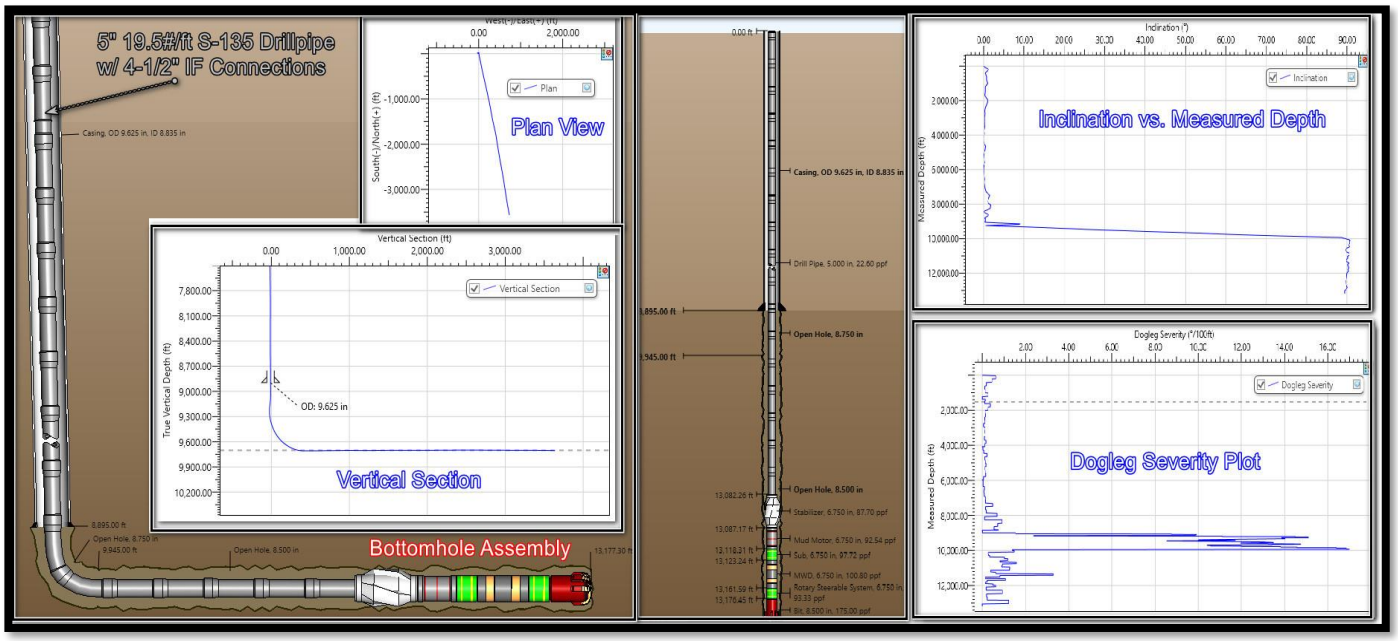

Figure 5a – Vertical and deviated schematic view of the drilling BHA. Plan view (top left) and vertical section view (bottom left) illustrate this well to be a simple 2D horizontal well. Dogleg severity (bottom right) and inclination (top right) plots are also shown. The well design had a planned build rate of 10°/100 ft, and the maximum dogleg experienced in the curve was less 17°/100 ft.

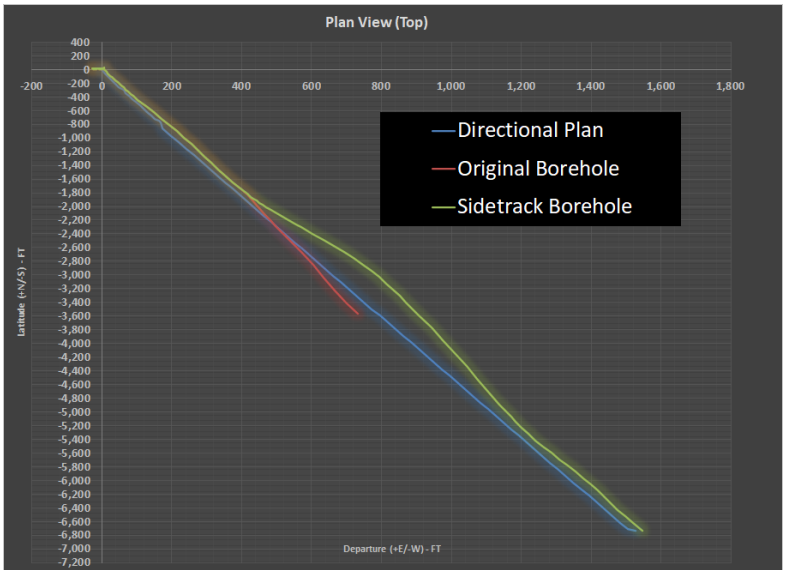

Figure 5b – The original interval shown in red was abandoned at 11,350 ft measured depth; the new sidetrack lateral (green) was successfully drilled to meet the original planned (blue) depth.

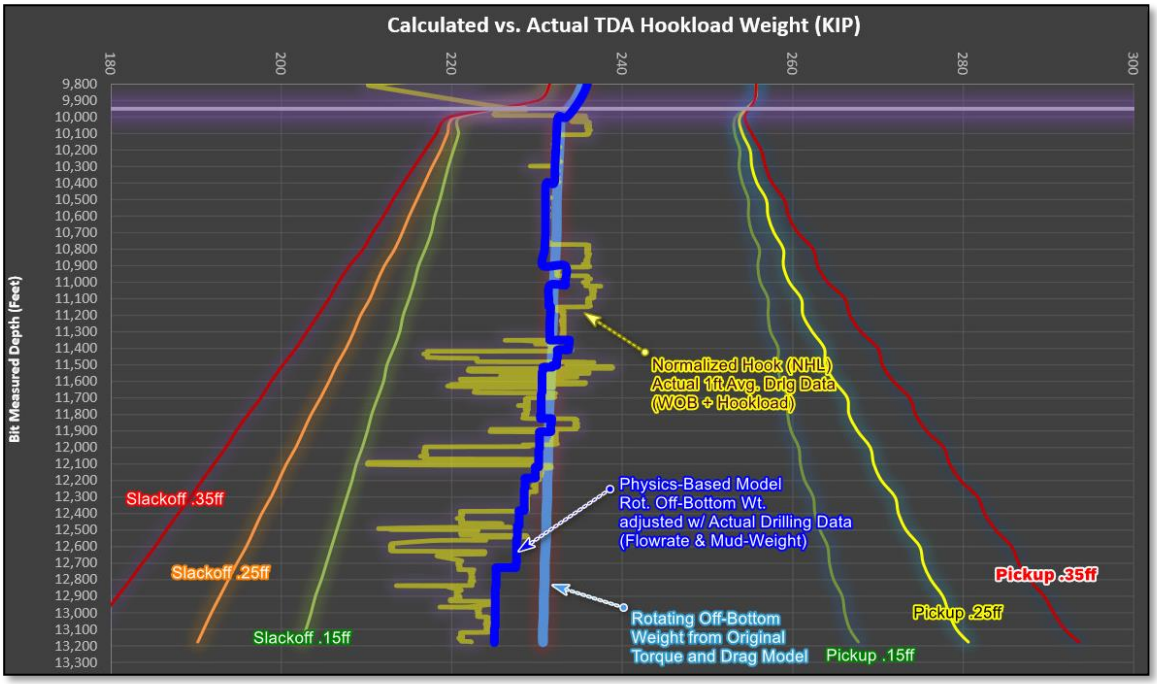

Figure 6 – Normalized hookload broomstick chart showing three friction-factor sensitivity curves for pickup and slack-off. Center light-blue curve is the rotating off-bottom weight, which slants backward slightly due to reduction in pipe tension at the surface. The borehole fully supports the BHA and pipe weight in the lateral due to the normal-force vector. Tension at the surface is primarily a result of changes in either flow rate or mud density. Addition of the drilling hookload and bit weight (WOB) while drilling presents normalized hookload, the yellow center line. The dark blue line in the center is the physics-based model of rotational weight adjusted with the actual drilling flow rate and fluid density. The delta between dark-blue and yellow lines indicates a bad zero setpoint tare that most likely led to bit weight error. It seems the calibration of the tare was good until about 10,700 ft. The ZSP used by the rig does not obey the general law of physics. Because the recalculated hookload based on actual flow rate and fluid density changed while drilling, it is clear to see that the rig made mistakes with taring the zero bit weight, which likely led to gross error in drilling parameters.

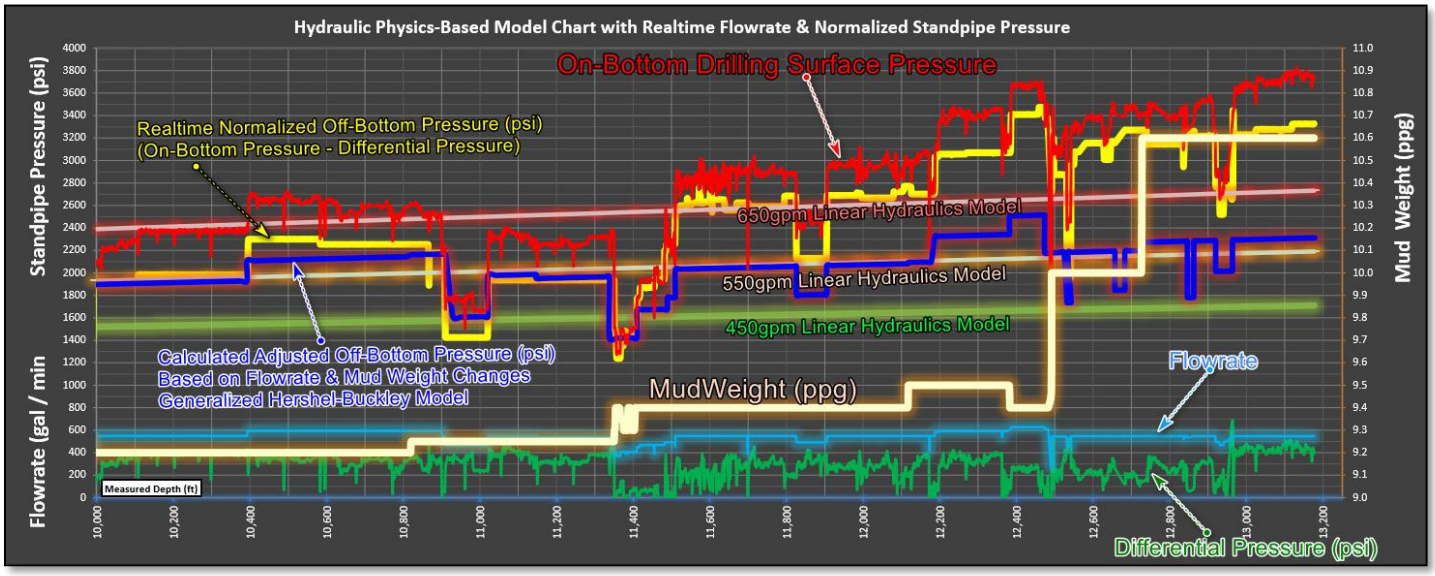

Figure 7 – The above chart includes three basic linear hydraulic models at 450 gpm, 550 gpm, and 650 gpm. Shown are the real-time differential pressure (dark green), flow rate (blue), mud weight (light yellow) and surface drilling pressure (red) as 1-ft average drilling data curves exported from the rigsite drilling data system. The surface drilling pressure and differential pressure move consistently; the ΔP increases or decreases, as does the surface pressure. However, subtracting the ΔP from the surface drilling pressure presents a new curve (dark yellow) called the real-time normalized off-bottom pressure. The normalized pressure clearly does not match the linear hydraulic curves. Because the flow rate and fluid density were not held constant while drilling, the linear models cannot be used effectively. The dark blue line is a curve recalculated after drilling using the actual drilling flow rate and fluid density from the rig data recording system. It is clear that the calibrated pressure setpoint becomes inconsistent as the well is deepened. This chart provides a good example of either the ZSP (zero set point) being in error or there is unusually high circulating pressure from inadequate hole cleaning, or a combination of both.

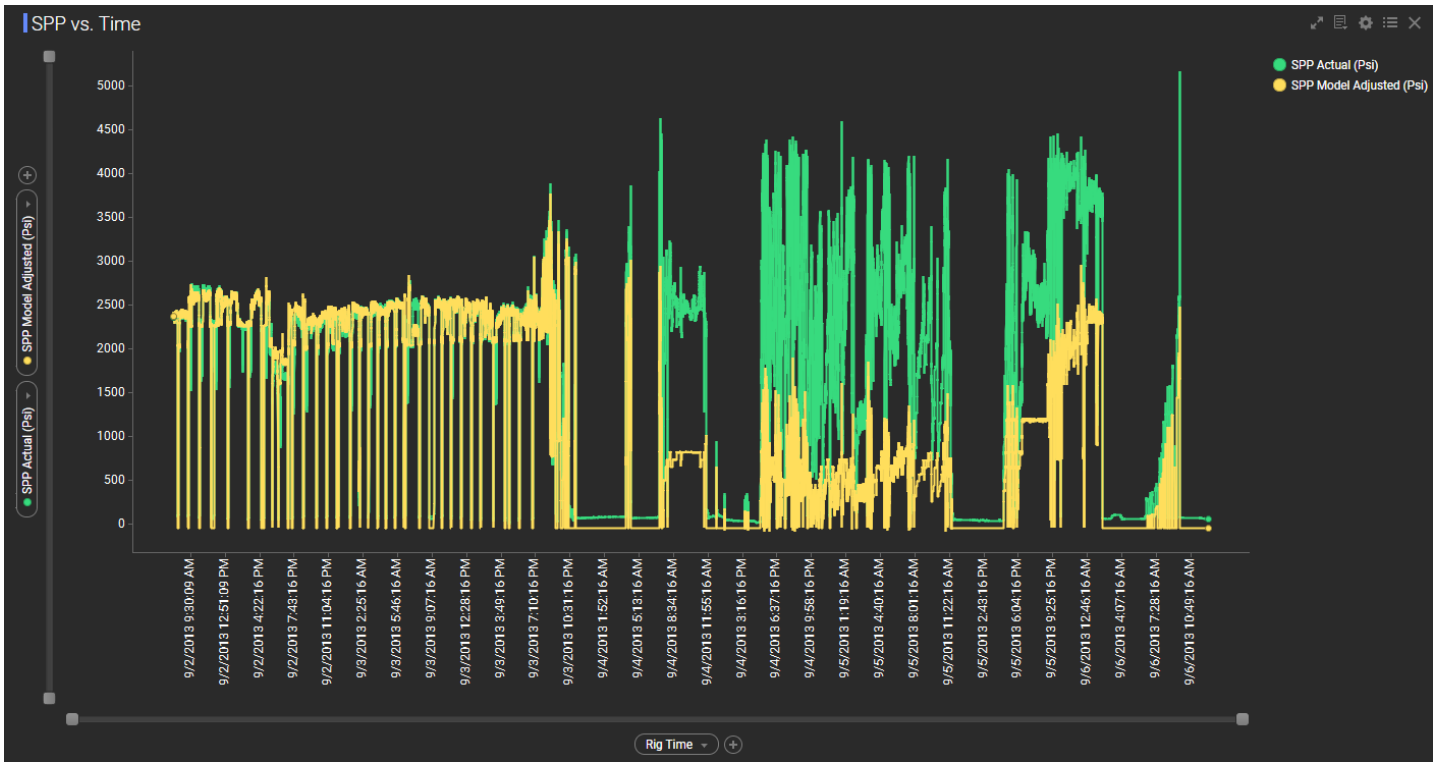

Figure 8 – Actual and modeled (using the new hydraulic tool) standpipe pressure vs. time.

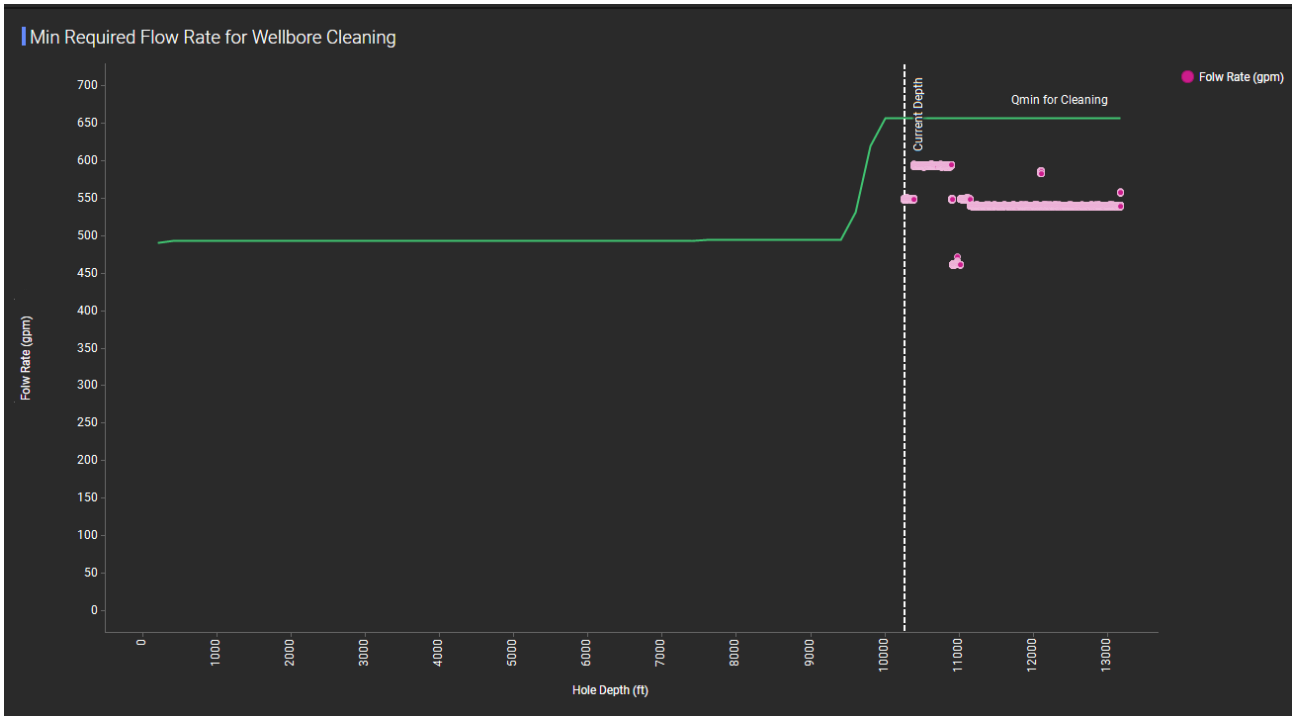

Figure 9 – Minimum required flow rate to clean the wellbore vs. depth. The green line indicates the minimum required flow rate, and the pink dots are the actual flow rates used in the field, which were significantly below the minimum required flow rate to clean the wellbore.

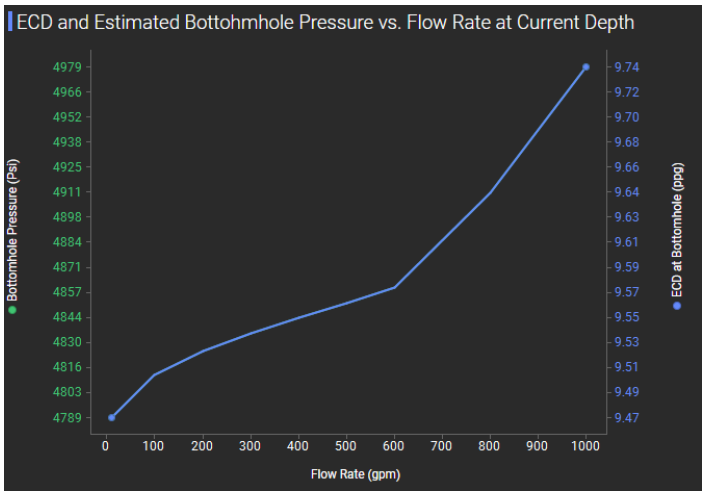

Figure 10 – Bottomhole pressure and ECD vs. flow rate. Increase in ECD and BHP is more prominent after 650 gpm.

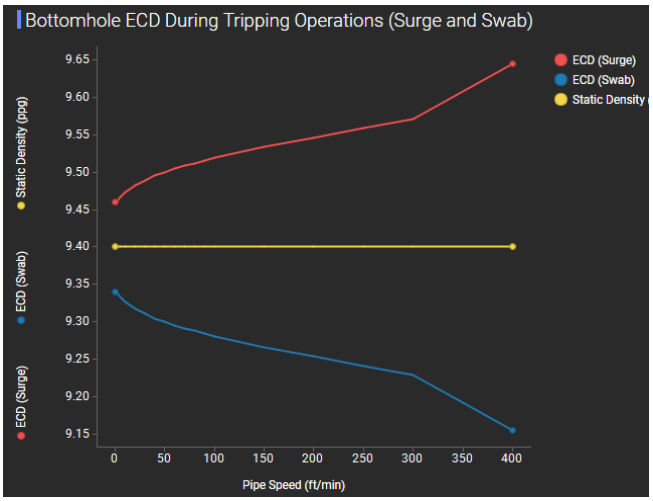

Figure 11 – Surge and swab ECD vs. the pipe movement speed at a certain depth.

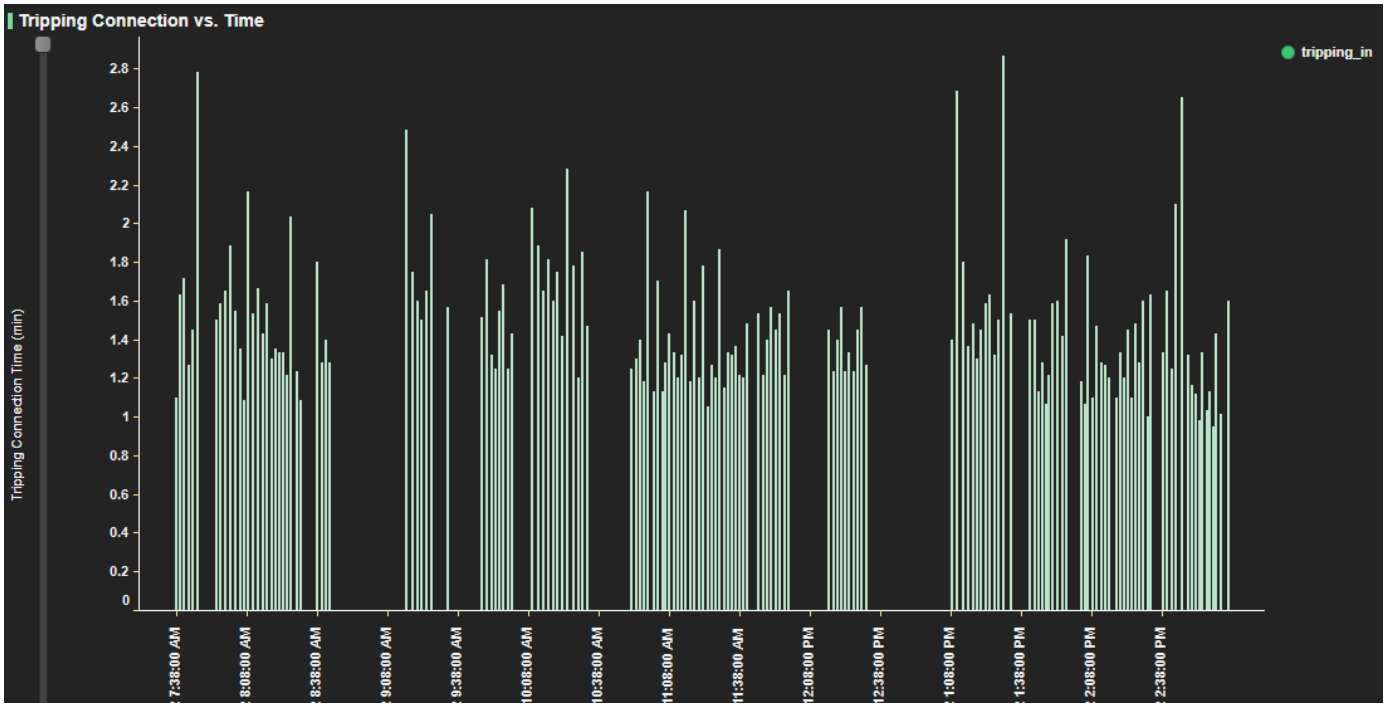

Figure 12 – Example of the tripping out connection time vs. time. The average pipe movement speed can be estimated from the connection time. A separate algorithm has been developed to obtain the connection time, which is not discussed here (see Karimi et al., 2019).